

Reactions in the Al–H–Cl System Studied by *ab Initio* Molecular Orbital and Density Functional Methods

Mark T. Swihart*

Department of Chemical Engineering, University at Buffalo (SUNY), Buffalo, New York 14260-4200

Laurent Catoire

Laboratoire de Combustion et Systèmes Réactifs (LCSR), CNRS, and University of Orleans, IC, av. de la recherche scientifique, 45071 Orleans Cedex 2, France

Received: September 28, 2000

High-level *ab initio* quantum chemical calculations have been used to investigate possible reactions in the Al–H–Cl system. Transition states or barrierless reaction paths have been identified for essentially all feasible reactions in this system involving a single aluminum atom. Structures, energies, and vibrational frequencies for reactants, products, and transition states in this system are presented. These results provide a basis for the estimation of reaction rate parameters for this system using transition state theory and related unimolecular reaction rate theories and thereby construct a reaction mechanism useful for detailed chemical kinetic modeling of aluminum combustion in HCl and chemical vapor deposition using AlCl₃ in H₂. In the few cases where previous experimental or theoretical results have been published, the present work is consistent with previous work.

Introduction

The gas-phase chemistry of the Al–H–Cl system is of interest in at least two contexts: (1) AlCl₃ can be used as a precursor for the deposition of aluminum-containing materials by CVD processes, often in the presence of H₂, and (2) aluminum is added to solid rocket propellant where it can react exothermically with the products of combustion of other fuels, including HCl, H₂O, CO, and CO₂. However, there is very little experimental information on elementary reactions in this system, or even on the thermochemistry of many of the species. To the best of our knowledge, no experiments concerning the combustion of Al particles in pure HCl have been reported in the open literature. A few reactions in this system have been studied experimentally^{1–3} or theoretically,^{4,5} but most of the possible reactions remain uninvestigated. We are using computational chemistry to explore possible reactions in this system and to calculate rate parameters for elementary gas-phase reactions. In recently published work,⁶ we used high-accuracy molecular orbital calculations to establish the thermochemistry of compounds in this system and of some oxygen, nitrogen, and carbon-containing aluminum compounds. On the basis of these results, we have identified possible reactions in the Al–H–Cl system and are applying transition state theory and unimolecular reaction rate theories to calculate rate parameters for these reactions. Molecular orbital calculations of transition state properties and reaction paths serve as inputs to these rate parameter calculations. For elementary reactions with an activation barrier, we have located transition states and computed their energies using high-accuracy compound methods for energy calculations, including the G-2, CBS-Q, and CBS-RAD methods. For simple bond-breaking reactions without an activation barrier in the exothermic direction, we have used density

functional theory calculations to evaluate the energy as a function of the breaking bond length. Conventional transition state theory, with tunneling corrections as necessary, is used to compute the rate parameters for bimolecular reactions. Unimolecular and recombination reactions are treated using RRKM theory and master equation calculations. Results of the molecular orbital calculations are presented in this paper, while computed kinetic parameters will be presented separately.⁷

Computational Methods

Four high-accuracy *ab initio* models for computational thermochemistry were applied to the aluminum compounds and transition states studied here. The first method was based on density functional theory calculations using the B3LYP functional. This functional employs Becke's gradient-corrected exchange functional,⁸ the Lee–Yang–Parr correlational functional,⁹ and three parameters fit to the original G-2 test set.¹⁰ The geometry optimization and frequency calculations for this method used the 6-31G(d) basis set. The energy at that geometry was then calculated using the 6-311+G(3df,2p) basis set. The second method used here was the CBS-Q complete basis set method of Ochterski et al.¹¹ This method employs the asymptotic convergence of pair natural orbital expansions to extrapolate to the second-order Møller–Plesset (MP2) complete basis set limit. The higher-order contributions are then evaluated using smaller basis sets. The third method used was the Gaussian-2 (G-2) model. This method approximates a quadratic configuration interaction calculation with a large basis set (QCISD-(T)/6-311+G(3df,2p)) by combining a series of smaller calculations and assuming the additivity of several components of the energy.^{12–14} All of the calculations were carried out using the Gaussian 94 computer program.¹⁵

Many of the species and transition states considered here have open-shell ground-state electronic configurations (one or more

* Corresponding author. E-mail: swihart@eng.buffalo.edu. Tel: (716) 645-2911, x. 2205. Fax: (716) 645-3822.

TABLE 1: Reactant, Product, and Transition-State Energies

species	total energy (hartrees) ^a				relative energy (kcal mol ⁻¹) ^b			
	B3LYP ^c	CBS-Q	G-2	CBS-RAD	B3LYP ^c	CBS-Q	G-2	CBS-RAD
AlH	-243.001271	-242.542997	-242.546190	-242.544989	0.0	0.0	0.0	0.0
Al ^d + H	-242.888857	-242.428515	-242.430950	-242.428486	70.5	71.8	72.3	73.1
AlCl	-702.741598	-701.808146	-701.800168	-701.807884	0.0	0.0	0.0	0.0
Al ^d + Cl ^d	-702.555447	-701.611935	-701.607923	-701.611879	116.8	123.1	120.6	123.0
AlH ₂	-243.580957	-243.117319	-243.118965	-243.117100	0.0	0.0	0.0	0.0
Al ^d + H ₂	-243.557108	-243.095127	-243.097652	-243.095061	15.0	13.9	13.4	13.8
AlH + H	-243.503427	-243.042815	-243.046190	-243.044807	48.7	46.8	45.7	45.4
AlH ₂ ↔ Al + H ₂ SP ^e	-243.517765			-243.051663	39.7			41.1
AlHCl	-703.300791	-702.362308	-702.353346	-702.362027	0.0	0.0	0.0	0.0
AlCl + H	-703.243754	-702.307964	-702.300168	-702.307702	35.8	34.1	33.4	34.1
Al ^d + HCl	-703.218823	-702.276112	-702.271471	-702.276047	51.4	54.1	51.4	54.0
AlH + Cl ^d	-703.171015	-702.227233	-702.224161	-702.229198	81.4	84.8	81.1	83.4
Al + HCl ↔ AlCl + H SP ^e	-703.219293	-702.274135	-702.262908	-702.269822	51.1	55.3	56.8	57.9
Al + HCl ↔ AlHCl SP ^e	-703.226833	-702.284301	-702.275298	-702.283424	46.4	49.0	49.0	49.3
Al–HCl complex	-703.226503	-702.281895	-702.276027	-702.281485	46.6	50.5	48.5	50.5
Al–ClH complex		-702.279034	-702.273953	-702.278719		52.3	49.8	52.3
AlCl ₂	-1163.016482	-1161.604454	-1161.585244	-1161.604014	0.0	0.0	0.0	0.0
AlCl + Cl ^d	-1162.911342	-1161.492382	-1161.478139	-1161.492093	66.0	70.3	67.2	70.2
Al ^d + Cl ₂	-1162.810259	-1161.388648	-1161.373501	-1161.388444	129.4	135.4	132.9	135.3
AlH ₃	-244.213664	-243.750511	-243.753945	-243.750143	0.0	0.0	0.0	0.0
AlH + H ₂	-244.171338	-243.709087	-243.712552	-243.711042	26.6	26.0	26.0	24.5
AlH ₂ + H	-244.083113	-243.617137	-243.618965	-243.616918	81.9	83.7	84.7	83.6
AlH + H ₂ ↔ AlH ₃ SP ^e	-244.115870			-243.652045	61.4			61.6
AlH ₂ Cl	-703.931955	-702.994383	-702.987800	-702.993963	0.0	0.0	0.0	0.0
AlCl + H ₂	-703.911664	-702.974236	-702.966530	-702.973937	12.7	12.6	13.3	12.6
AlH + HCl	-703.833052	-702.890072	-702.886371	-702.892028	62.1	65.5	63.6	64.0
AlHCl + H	-703.802947	-702.862126	-702.853346	-702.861845	81.0	83.0	84.4	82.9
AlH ₂ + Cl ^d	-703.749363	-702.800217	-702.795598	-702.799971	114.6	121.8	120.6	121.7
AlH ₂ Cl ↔ AlH + HCl SP ^e	-703.824547			-702.878649	67.4			72.4
AlH ₂ Cl ↔ AlCl + H ₂ SP ^e	-703.814280			-702.875799	73.8			74.1
AlHCl + H ↔ AlH + HCl SP ^e	-703.799626			-702.856708	83.0			86.1
AlHCl ₂	-1163.647904	-1162.236874	-1162.220233	-1162.236393	0.0	0.0	0.0	0.0
AlCl + HCl	-1163.573379	-1162.155221	-1162.140349	-1162.154923	46.8	51.2	50.1	51.1
AlCl ₂ + H	-1163.518638	-1162.104272	-1162.085244	-1162.103832	81.1	83.2	84.7	83.2
AlHCl + Cl ^d	-1163.470535	-1162.046544	-1162.031317	-1162.046236	111.3	119.4	118.5	119.3
AlH + Cl ₂	-1163.424488	-1162.002608	-1161.988401	-1162.004425	140.2	147.0	145.5	145.6
AlCl + HCl ↔ AlCl ₂ + H SP ^e	-1163.517761			-1162.102112	81.7			84.3
AlCl + HCl ↔ AlHCl ₂ SP ^e	-1163.543944			-1162.124689	65.2			70.1
AlCl ₃	-1623.358956	-1621.475524	-1621.448747	-1621.474935	0.0	0.0	0.0	0.0
AlCl ₂ + Cl ^d	-1623.184888	-1621.287352	-1621.261877	-1621.286885	109.2	118.1	117.3	118.0
AlCl + Cl ₂	-1623.164815	-1621.267757	-1621.242379	-1621.267320	121.8	130.4	129.5	130.3
AlCl ₂ + Cl ↔ AlCl + Cl ₂ SP ^e				-1621.280152				122.2
AlH ₂ + H ₂	-244.751024	-244.283409	-244.285327	-244.283153	0.0	0.0	0.0	0.0
AlH ₄	-244.734780	-244.262876	-244.265198	-244.261715	10.2	12.9	12.6	13.5
AlH ₃ + H	-244.715820	-244.250329	-244.253945	-244.249961	22.1	20.8	19.7	20.8
AlH ₂ + H ₂ ↔ AlH ₃ + H SP ^e	-244.715829	-244.247147	-244.249302	-244.245560	22.1	22.8	22.6	23.6
AlH ₂ + H ₂ ↔ AlH ₄ SP ^e	-244.736355	-244.266541	-244.268343	-244.265649	9.2	10.6	10.7	11.0
AlH ₃ + H ↔ AlH ₄ SP ^e		-244.254602	-244.257584	-244.252051		18.1	17.4	19.5
AlHCl + H ₂	-704.470858	-703.528398	-703.519708	-703.528080	0.0	0.0	0.0	0.0
AlH ₃ Cl	-704.447696	-703.502535	-703.495091	-703.500739	14.5	16.2	15.4	17.2
AlH ₂ Cl + H	-704.434111	-703.494201	-703.487800	-703.493781	23.1	21.5	20.0	21.5
AlH ₂ + HCl	-704.412739	-703.464394	-703.459146	-703.464139	36.5	40.2	38.0	40.1
AlH ₃ + Cl ^d	-704.383408	-703.434747	-703.431916	-703.434352	54.9	58.8	55.1	58.8
AlH ₂ Cl + H ↔ AlHCl + H ₂ SP ^e	-704.433770	-703.491033	-703.483040	-703.489335	23.3	23.4	23.0	24.3
AlH ₃ Cl ↔ AlHCl + H ₂ SP ^e	-704.446321	-703.502294	-703.493861	-703.501372	15.4	16.4	16.2	16.8
AlH ₂ + HCl ↔ AlH ₂ Cl + H SP ^e	-704.413667	-703.467889	-703.460413	-703.466837	35.9	38.0	37.2	38.4
AlH ₂ Cl + H ↔ AlH ₃ Cl SP ^e		-703.498512	-703.491043	-703.495881		18.8	18.0	20.2
AlCl ₂ + H ₂	-1164.186549	-1162.770544	-1162.751606	-1162.770067	0.0	0.0	0.0	0.0
AlH ₂ Cl ₂	-1164.161278	-1162.740694 ^f	-1162.725035 ^f	-1162.739092	15.9	18.7 ^f	16.7 ^f	19.4
AlHCl ₂ + H	-1164.150060	-1162.736692	-1162.720233	-1162.736211	22.9	21.2	19.7	21.2
AlHCl + HCl	-1164.132573	-1162.709383	-1162.693527	-1162.709066	33.9	38.4	36.4	38.3
AlH ₂ Cl + Cl ^d	-1164.101699	-1162.678619	-1162.665771	-1162.678172	53.2	57.7	53.9	57.7
AlH ₂ + Cl ₂	-1164.004174	-1162.576930	-1162.561176	-1162.576536	114.4	121.5	119.5	121.4
AlHCl ₂ + H ↔ AlCl ₂ + H ₂ SP ^e	-1164.149246	-1162.733438	-1162.715378	-1162.731684	23.4	23.3	22.7	24.1
AlHCl ₂ + H ↔ AlHCl + HCl SP ^e	-1164.124711	-1162.700819	-1162.681934	-1162.699763	38.8	43.8	43.7	44.1
AlH ₂ Cl ₂ ↔ AlCl ₂ + H ₂ SP ^e	-1164.154273			-1162.735171	20.3			21.9
AlHCl ₂ + H ↔ AlH ₂ Cl ₂ SP ^e				-1162.738144				20.0
AlCl ₃ + H	-1623.861112	-1621.975342	-1621.948747	-1621.974753	0.0	0.0	0.0	0.0
AlCl ₂ + HCl	-1623.848263	-1621.951529	-1621.925425	-1621.951053	8.1	14.9	14.6	14.9
AlHCl ₂ + Cl ^d	-1623.816310	-1621.919772	-1621.896866	-1621.919264	28.1	34.9	32.6	34.8
AlHCl + Cl ₂	-1623.724009	-1621.821919	-1621.795557	-1621.821463	86.0	96.3	96.1	96.2
AlCl ₃ + H ↔ AlCl ₂ + HCl SP ^e	-1623.837378	-1621.940108	-1621.912098	-1621.939547	14.9	22.1	23.0	22.1

TABLE 1 (Continued)

species	total energy (hartrees) ^a				relative energy (kcal mol ⁻¹) ^b			
	B3LYP ^c	CBS-Q	G-2	CBS-RAD	B3LYP ^c	CBS-Q	G-2	CBS-RAD
AlHCl ₂ + Cl ↔ AlCl ₂ + HCl SP ^e		-1621.935467	-1621.908349	-1621.937063		25.0	25.4	23.7
AlCl ₄	-2083.558766	-2081.192201	-2081.152158	-2081.190707	0.0	0.0	0.0	0.0
AlCl ₃ + Cl ^d	-2083.528700	-2081.159760	-2081.126718	-2081.159144	18.9	20.4	16.0	19.8
AlCl ₂ + Cl ₂	-2083.439699	-2081.064065	-2081.027455	-2081.063450	74.7	80.4	78.3	79.9

^a Total energy at 0 K, including zero-point energy. ^b Energy relative to the lowest-energy configuration of the same atoms. ^c B3LYP/6-311+G(3df,2p)//B3LYP/6-31G(d) energy plus zero-point energy calculated from the B3LYP/6-31G(d) frequencies, scaled by 0.9804. ^d Energies of Al and Cl atoms include experimental spin-orbit corrections of 0.2136 and 0.8396 kcal/mol, respectively. ^e SP indicates a first-order saddle point on the reaction path between the given reactant(s) and product(s). ^f This structure is a first-order saddle point at the UHF/6-31G(d) level but a minimum at the UMP2/6-31G(d) level. The imaginary frequency has been ignored in computing the zero-point energy from the UHF/6-31G(d) frequencies.

TABLE 2: Geometric Parameters

species	symmetry group	figure 1 part	QCISD/6-31G(d) geometric parameters ^a (Å and deg)
AlH	<i>C</i> _{∞v}		<i>R</i> (Al-H) 1.67
AlCl	<i>C</i> _{∞v}		<i>R</i> (Al-Cl) 2.14
AlH ₂	<i>C</i> _{2v}		<i>R</i> (Al-H) 1.61, <i>A</i> (H-Al-H) 118
AlH ₂ ↔ Al + H ₂ SP ^b	<i>C</i> _s	a	<i>R</i> (Al-H ₁) 1.80, <i>R</i> (Al-H ₂) 1.75, <i>A</i> (H ₁ -Al-H ₂) 58
AlHCl	<i>C</i> _s		<i>R</i> (Al-H) 1.61, <i>R</i> (Al-Cl) 2.12, <i>A</i> (H-Al-Cl) 116
Al + HCl ↔ AlCl + H SP ^b	<i>C</i> _s	b	<i>R</i> (Al-Cl) 2.37, <i>R</i> (Cl-H) 1.50, <i>A</i> (Al-Cl-H) 133
Al + HCl ↔ AlHCl SP ^b	<i>C</i> _s	c	<i>R</i> (Al-H) 1.96, <i>R</i> (Al-Cl) 2.77, <i>A</i> (H-Al-Cl) 30.6
Al-HCl cluster	<i>C</i> _{∞v}	d	<i>R</i> (Al-H) 3.04, <i>R</i> (H-Cl) 1.29
Al-ClH cluster	<i>C</i> _s	e	<i>R</i> (Al-Cl) 3.74, <i>R</i> (Cl-H) 1.29, <i>A</i> (Al-Cl-H) 91
AlCl ₂	<i>C</i> _{2v}		<i>R</i> (Al-Cl) 2.10, <i>A</i> (Cl-Al-Cl) 119
AlH ₃	<i>D</i> _{3h}		<i>R</i> (Al-H) 1.60
AlH + H ₂ ↔ AlH ₃ SP ^b	<i>C</i> _s	f	<i>R</i> (Al-H ₁) 1.59, <i>R</i> (Al-H ₂) 1.85, <i>R</i> (Al-H ₃) 1.60, <i>A</i> (H ₁ -Al-H ₂) 72, <i>A</i> (H ₂ -Al-H ₃) 53
AlH ₂ Cl	<i>C</i> _{2v}		<i>R</i> (Al-H) 1.59, <i>R</i> (Al-Cl) 2.10, <i>A</i> (H-Al-H) 125
AlH ₂ Cl ↔ AlCl + H ₂ SP ^b	<i>C</i> _s	g	<i>R</i> (Al-H ₁) 1.59, <i>R</i> (Al-H ₂) 1.90, <i>R</i> (Al-Cl) 2.10, <i>A</i> (H ₁ -Al-H ₂) 49, <i>A</i> (H ₂ -Al-Cl) 95
AlH ₂ Cl ↔ AlH + HCl SP ^b	<i>C</i> _s	h	<i>R</i> (Al-H ₁) 1.61, <i>R</i> (Al-H ₂) 1.75, <i>R</i> (Al-Cl) 2.59, <i>A</i> (H ₂ -Al-Cl) 37, <i>A</i> (H ₁ -Al-Cl) 101
AlHCl + H ↔ AlH ₂ + HCl SP ^b	<i>C</i> _s	i	<i>R</i> (Al-H ₁) 1.63, <i>R</i> (Al-Cl) 2.24, <i>R</i> (Cl-H ₂) 1.67, <i>A</i> (H ₁ -Al-Cl) 109, <i>A</i> (Al-Cl-H ₂) 143
AlHCl ₂	<i>C</i> _{2v}		<i>R</i> (Al-Cl) 2.09, <i>R</i> (Al-H) 1.58, <i>A</i> (Cl-Al-Cl) 119
AlCl + HCl ↔ AlHCl ₂ SP ^b	<i>C</i> _s	j	<i>R</i> (Al-Cl ₁) 2.10, <i>R</i> (Al-Cl ₂) 2.50, <i>R</i> (Al-H) 1.73, <i>A</i> (Cl ₂ -Al-H) 41, <i>A</i> (Cl ₁ -Al-Cl ₂) 108
AlCl + HCl ↔ AlCl ₂ + H SP ^b	<i>C</i> _s	k	<i>R</i> (Al-Cl ₁) 2.11, <i>R</i> (Al-Cl ₂) 2.23, <i>R</i> (Cl ₂ -H) 1.77, <i>A</i> (Cl ₁ -Al-Cl ₂) 116, <i>A</i> (Al-Cl ₂ -H) 155.
AlCl ₃	<i>D</i> _{3h}		<i>R</i> (Al-Cl) 2.08
AlCl ₂ + Cl ↔ AlCl + Cl ₂ SP ^b	<i>C</i> _s	l	<i>R</i> (Al-Cl ₁) 2.12, <i>R</i> (Al-Cl ₂) 2.60, <i>R</i> (Cl ₂ -Cl ₃) 2.14, <i>A</i> (Cl ₁ -Al-Cl ₂) 125, <i>A</i> (Al-Cl ₂ -Cl ₃) 163
AlH ₄	<i>C</i> _{2v}	m	<i>R</i> (Al-H ₁) 1.59, <i>R</i> (Al-H ₂) 1.71, <i>A</i> (H ₁ -Al-H ₁) 127, <i>A</i> (H ₁ -Al-H ₂) 114, <i>A</i> (H ₂ -Al-H ₂) 52
AlH ₂ + H ₂ ↔ AlH ₃ + H SP ^b	<i>C</i> _{2v}	n	<i>R</i> (Al-H ₁) 1.60, <i>R</i> (Al-H ₂) 1.73, <i>R</i> (H ₂ -H ₃) 1.20, <i>A</i> (H ₁ -Al-H ₂) 120
AlH ₂ + H ₂ ↔ AlH ₄ SP ^b	<i>C</i> _{2v}	o	<i>R</i> (Al-H ₁) 1.59, <i>R</i> (Al-H ₂) 1.71, <i>A</i> (H ₁ -Al-H ₁) 132, <i>A</i> (H ₁ -Al-H ₂) 112, <i>A</i> (H ₂ -Al-H ₂) 41
AlH ₃ + H ↔ AlH ₄ SP ^b	<i>C</i> _s	p	<i>R</i> (Al-H ₁) 1.50, <i>R</i> (Al-H ₂) 1.62, <i>R</i> (Al-H ₃) 2.11, <i>A</i> (H ₁ -Al-H ₂) 119, <i>A</i> (H ₂ -Al-H ₃) 68
AlH ₃ Cl	<i>C</i> _s	q	<i>R</i> (Al-H ₁) 1.71, <i>R</i> (Al-H ₂) 1.58, <i>R</i> (Al-Cl) 2.10, <i>A</i> (H ₁ -Al-H ₁) 58, <i>A</i> (H ₁ -Al-H ₂) 118, <i>A</i> (H ₁ -Al-Cl) 113
AlH ₂ Cl + H ↔ AlHCl + H ₂ SP ^b	<i>C</i> _s	r	<i>R</i> (Al-H ₁) 1.59, <i>R</i> (Al-Cl) 2.11, <i>R</i> (Al-H ₂) 1.71, <i>R</i> (H ₂ -H ₃) 1.21, <i>A</i> (H ₁ -Al-Cl) 117, <i>A</i> (H ₁ -Al-H ₂) 125, <i>A</i> (Al-H ₂ -H ₃) 179
AlH ₂ + HCl ↔ AlH ₂ Cl + H SP ^b	<i>C</i> _s	s	<i>R</i> (Al-H ₁) 1.59, <i>R</i> (Al-H ₂) 1.97, <i>R</i> (H ₂ -Cl) 1.41, <i>A</i> (H ₁ -Al-H ₁), 126, <i>A</i> (H ₁ -Al-H ₂) 114, <i>A</i> (Al-H ₂ -Cl ₃) 97
AlH ₃ Cl ↔ AlHCl + H ₂ SP ^b	<i>C</i> ₁	t	<i>R</i> (Al-H ₁) 1.58, <i>R</i> (Al-Cl) 2.10, <i>R</i> (Al-H ₂) 1.67, <i>R</i> (Al-H ₃) 1.77, <i>A</i> (H ₁ -Al-Cl) 128, <i>A</i> (H ₁ -Al-H ₂) 118, <i>A</i> (H ₁ -Al-H ₃) 109, <i>A</i> (H ₂ -Al-H ₃) 35, <i>A</i> (H ₂ -Al-Cl) 110
AlH ₂ Cl + H ↔ AlH ₃ Cl SP ^b	<i>C</i> ₁	u	<i>R</i> (Al-H ₁) 1.61, <i>R</i> (Al-H ₂) 1.59, <i>R</i> (Al-H ₃) 2.01, <i>R</i> (Al-Cl) 2.11, <i>A</i> (H ₁ -Al-H ₂) 124, <i>A</i> (H ₁ -Al-H ₃) 68, <i>A</i> (H ₁ -Al-Cl) 117, <i>R</i> (H ₂ -Al-H ₃) 106, <i>R</i> (H ₂ -Al-Cl) 119
AlH ₂ Cl ₂	<i>C</i> _{2v}	v	<i>R</i> (Al-H) 1.70, <i>R</i> (Al-Cl) 2.09, <i>A</i> (H-Al-H) 63, <i>A</i> (H-Al-Cl) 115
AlHCl ₂ + H ↔ AlCl ₂ + H ₂ SP ^b	<i>C</i> _{2v}	w	<i>R</i> (Al-Cl) 2.09, <i>R</i> (Al-H ₁) 1.69, <i>R</i> (H ₁ -H ₂) 1.22, <i>A</i> (Cl-Al-H ₁) 121
AlHCl ₂ + H ↔ AlHCl + HCl SP ^b	<i>C</i> ₁	x	<i>R</i> (Al-H ₁) 1.59, <i>R</i> (Al-Cl ₁) 2.11, <i>R</i> (Al-Cl ₂) 2.26, <i>R</i> (Cl ₂ -H ₂) 1.52, <i>A</i> (H ₁ -Al-Cl ₁) 120, <i>A</i> (H ₁ -Al-Cl ₂) 115, <i>A</i> (Cl ₁ -Al-Cl ₂) 114, <i>A</i> (Al-Cl ₂ -H ₂) 135, <i>D</i> (H ₁ -Al-Cl ₂ -H ₂) 67
AlH ₂ Cl ₂ ↔ AlCl ₂ + H ₂ SP ^b	<i>C</i> _s	y	<i>R</i> (Al-Cl) 2.09, <i>R</i> (Al-H ₁) 1.64, <i>R</i> (Al-H ₂) 1.86, <i>A</i> (Cl-Al-H ₁) 117, <i>A</i> (Cl-Al-H ₂) 108, <i>A</i> (H ₁ -Al-H ₂) 36
AlHCl ₂ + H ↔ AlH ₂ Cl ₂ SP ^b	<i>C</i> _s	z	<i>R</i> (Al-Cl) 2.09, <i>R</i> (Al-H ₁) 1.61, <i>R</i> (Al-H ₂) 1.92, <i>A</i> (Cl-Al-H ₁) 119, <i>A</i> (Cl-Al-H ₂) 106, <i>A</i> (H ₁ -Al-H ₂) 70
AlCl ₃ + H ↔ AlCl ₂ + HCl SP ^b	<i>C</i> _s	a'	<i>R</i> (Al-Cl ₁) 2.10, <i>R</i> (Al-Cl ₂) 2.26, <i>R</i> (Cl ₂ -H) 1.54, <i>A</i> (Cl ₁ -Al-Cl ₁) 119, <i>A</i> (Cl ₁ -Al-Cl ₂) 115, <i>A</i> (Al-Cl ₂ -H) 139
AlHCl ₂ + Cl ↔ AlCl ₂ + HCl SP ^b	<i>C</i> _{2v}	b'	<i>R</i> (Al-Cl ₁) 2.08, <i>R</i> (Al-H) 1.68, <i>R</i> (H-Cl ₂) 1.71, <i>A</i> (Cl ₁ -Al-H) 119
AlCl ₄	<i>C</i> _{2v}	c'	<i>R</i> (Al-Cl ₁) 2.09, <i>R</i> (Al-Cl ₂) 2.23, <i>A</i> (Cl ₁ -Al-Cl ₁) 120, <i>A</i> (Cl ₁ -Al-Cl ₂) 113
H ₂	<i>D</i> _{∞h}		<i>R</i> (H-H) 0.75
HCl	<i>C</i> _{∞v}		<i>R</i> (H-Cl) 1.29
Cl ₂	<i>D</i> _{∞h}		<i>R</i> (Cl-Cl) 2.03

^a *R*(A-B) indicates the distance between atoms A and B, *A*(A-B-C) indicates the A-B-C bond angle, and *D*(A-B-C-D) indicates the dihedral angle between A and D about the B-C bond. ^b SP indicates a first-order saddle point on the reaction path between the given reactant(s) and product(s).

unpaired electrons). All of the above methods use spin-unrestricted wave functions for open-shell species. These are not necessarily eigenfunctions of the spin-squared operator (S^2) and, therefore, do not yield pure doublet, triplet, etc. states. They may be contaminated by the states of higher-spin multiplicity. This spin contamination leads to values of $\langle S^2 \rangle$ that are greater than those of the pure spin states (i.e., $\langle S^2 \rangle$ greater than 0.75 for doublets, greater than 2.0 for triplets, etc.). For species with mild spin contamination ($\langle S^2 \rangle$ within 0.05 or so of the value for the pure spin state), the above methods were found by Mayer et al.¹⁶ to perform well. However, for more severely spin-contaminated wave functions, they do not give reliable energies. The effect of spin contamination on computed energies is discussed in more detail by Mayer et al.¹⁶ In addition, for some of the transition states studied here that are nominally closed-shell species, the restricted Hartree–Fock wave function was found to be unstable with respect to becoming unrestricted. In other cases, no transition state was found at the restricted Hartree–Fock level, or one was found that was qualitatively different from those found at higher levels or at the unrestricted Hartree–Fock level. In these cases, the CBS-Q and G-2 methods could not be used, since they are based on restricted Hartree–Fock methods for closed-shell species. Of course, the restricted calculations could be replaced with their unrestricted counterparts, but then it is questionable whether the result can still be called a CBS-Q or G-2 calculation. Therefore, the CBS-RAD method, recommended by Mayer et al.¹⁶ for computing high-accuracy energies of free radicals, was also applied to all of the molecules and transition states considered here. This is a variant of the CBS-Q method, in which the geometry optimization and frequency calculation are done at the QCISD/6-31G(d) level of theory, and the larger QCISD energy calculation is replaced by a coupled-cluster (CCSD(T)) calculation. This procedure was shown by Mayer et al.¹⁶ to give more accurate energies than the G-2 or CBS-Q methods for spin-contaminated radical species. In the CBS-RAD method, we used unrestricted wave functions for all species, including nominally closed-shell species. In most cases, for the closed-shell species, pure singlet states were obtained ($\langle S^2 \rangle = 0$), but for several of the transition states whose wave functions had RHF to UHF instabilities, somewhat spin-contaminated wave functions were obtained. In general, the CBS-RAD results were consistent with the CBS-Q and G-2 results. Chuang et al.¹⁷ studied the ability of single-reference methods to predict the properties of open-shell transition states and found that unrestricted quadratic configuration interaction (UQCISD) performed much better than unrestricted second-order Møller–Plesset perturbation theory (UMP2) in predicting transition state geometries and that it performed nearly as well as coupled-cluster methods (UCCSD and variants on it). We therefore expect that the UQCISD/6-31G(d) geometry optimizations and frequency calculations performed as part of the CBS-RAD method will provide more reliable geometries and frequencies than the other methods used here.

Results and Discussion

Computed energies of reactants, products, and transition states for possible reactions in the Al–H–Cl system are given in Table 1. Blank entries in the table indicate that a particular method was not applicable to a particular structure. The reasons for this are given below. We have previously reported heats of formation computed from these results for many of the stable species,⁶ but none of the transition state properties have been previously presented. Allendorf and co-workers^{18,19} have previously presented heats of formation of several of these species based on G-2 calculations. Table 2 presents the bond lengths and angles

needed to specify the geometry of each species. Selected molecules and transition states are illustrated in Figure 1. Table 3 presents the computed vibrational frequencies and moments of inertia for each of the species included in Table 1. The QCISD/6-31G(d) frequencies have been scaled by 0.9537, as recommended by Scott and Radom.²⁰ Note that a different scaling factor (0.9776) was used for the zero-point energy, also as recommended by Scott and Radom.²⁰ The numbers given in Table 1 are illustrated in schematic energy diagrams in Figure 2. This figure also shows the many reaction paths that have no energetic barrier and for which, therefore, no transition state properties are given in Table 1. Possible reactions for each stoichiometry— $\text{AlH}_x\text{Cl}_{2-x}$ ($x = 0-2$), $\text{AlH}_x\text{Cl}_{3-x}$ ($x = 0-3$), and $\text{AlH}_x\text{Cl}_{4-x}$ ($x = 0-4$)—are discussed individually below. In the tables and in Figure 1, we have included information on structures that are first-order saddle points at some levels of theory even when at the highest levels of theory used these structures become significantly lower in energy than the reactants and would therefore, in the context of variational transition state theory, not be transition states.

In this study, we have considered only reactions involving a single aluminum atom and five or fewer total atoms. We have not considered processes involving dimers of $\text{AlH}_x\text{Cl}_{3-x}$ that are known to exist in the gas phase at moderate temperatures, nor have we considered processes involving complexes such as $\text{AlCl}_3\cdot\text{HCl}$. The binding energy of the $\text{AlCl}_3\cdot\text{HCl}$ complex was computed by Senger and Radom²¹ to be about 8 kcal/mol. The binding energy for the AlCl_3 dimer is about 30 kcal/mol.²² Thus, a complete model of reactions in the Al–H–Cl system would need to include such processes to be applicable at temperatures below about 1000 K, where such complex formation can be significant. If the only possible reactions are reversible complex formations, then this will not add much to the chemistry. However, if the complexes can rearrange and decompose to a pair of compounds other than that from which they formed, processes proceeding through such complexes may be important. In any case, the investigation of such complexes and their reactions goes beyond the scope of the present study.

AlH₂. The potential surface for AlH_2 is shown schematically in Figure 2a. Decomposition of AlH_2 to $\text{AlH} + \text{H}$ is a simple bond-breaking reaction that is barrierless in the reverse direction. Decomposition of AlH_2 to $\text{Al} + \text{H}_2$ is thermodynamically preferable to decomposition to $\text{AlH} + \text{H}$ but has approximately the same energetic barrier to reaction. Since decomposition to $\text{Al} + \text{H}_2$ will proceed through a tight transition state while decomposition to $\text{AlH} + \text{H}$ proceeds through a loose transition state, decomposition to $\text{AlH} + \text{H}$ can be expected to be faster. The transition state for the decomposition of AlH_2 to $\text{Al} + \text{H}_2$ could not be located at the HF/6-31G(d) level, and therefore, no CBS-Q or G-2 results are presented for this structure. There is no energetic barrier for direct H abstraction from AlH by H. This was confirmed by conducting scans of the potential surface at the HF/6-31G(d) and B3LYP/6-31G(d) levels and identifying a barrierless path from $\text{AlH} + \text{H}$ to $\text{Al} + \text{H}_2$.

AlHCl. The potential surface for AlHCl is shown schematically in Figure 2b. The $\text{Al} + \text{HCl}$ reaction has been studied both experimentally and theoretically. In high-temperature fast-flow reactor studies, Rogowski et al.² measured a rate constant of $1.5 \times 10^{-10} \exp(-800/T) \text{ cm}^3 \text{ molecule}^{-1} \text{ s}^{-1}$. Both Sakai⁴ and Fängström et al.⁵ have studied this reaction using ab initio methods. Sakai considered only the insertion reaction to give AlHCl , while Fängström et al. also considered the Cl atom transfer to give $\text{AlCl} + \text{H}$. These two studies agree with the present result that Al and HCl can form two weakly bound

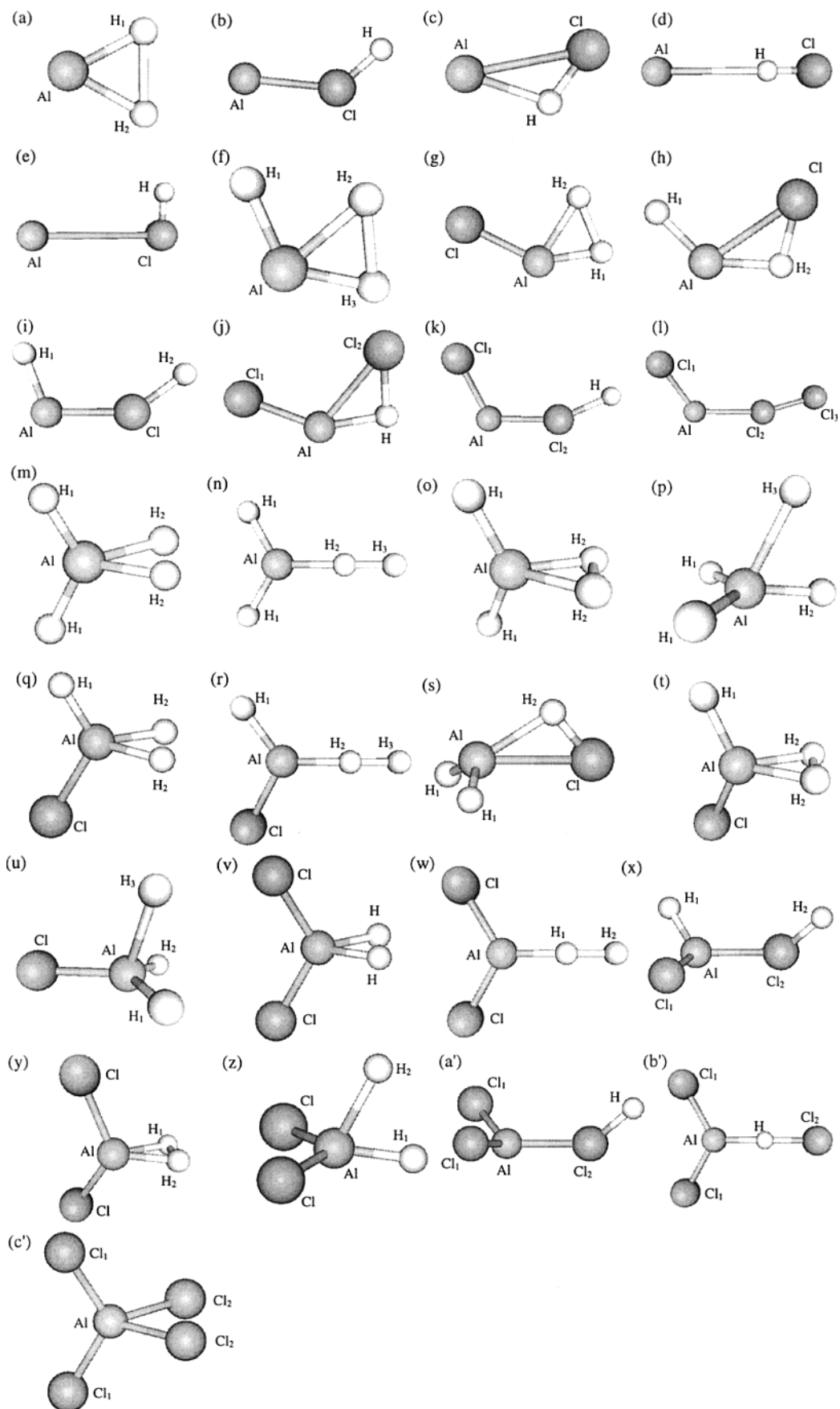


Figure 1. Structures of the selected molecules (potential energy surface minima) and first-order saddle points investigated here.

addition complexes, a linear Al–HCl structure, and a bent Al–ClH structure. As found by Fångström et al., the bent Al–ClH cluster is not present at the B3LYP/6-31G(d) level. The

transition state leading to AlHCl is slightly higher in energy than the addition complexes if only electronic energy is considered. However, inclusion of zero-point energy and

TABLE 3: Vibrational Frequencies and Moments of Inertia^a

species	scaled QCISD/6-31G(d) vibrational frequencies (cm ⁻¹)								moments of inertia (amu Å ²)			
AlH	1596									2.7		
AlCl	473									69.8		
AlH ₂	729	1750	1790							1.3	3.9	5.1
AlH ₂ ↔ Al + H ₂ SP ^b	-4003	758	1346							1.5	4.5	6.0
AlHCl	495	552	1734							2.0	71.9	73.9
Al + HCl ↔ AlCl + H SP ^b	-2836	285	470							1.2	89.4	90.5
Al + HCl ↔ AlHCl SP ^b	-946	200	1063							1.0	117	118
Al–HCl cluster	61	201	201	2699						287		
Al–ClH cluster	42	107	2843							1.6	215	217
AlCl ₂	148	451	567							22.3	230	252
AlH ₃	671	751	751	1834	1850	1850				3.9	3.9	7.7
AlH + H ₂ ↔ AlH ₃ SP ^b	-917	309	678	1025	1808	1858				3.6	4.7	8.2
AlH ₂ Cl	500	514	577	747	1871	1891				4.0	74.6	78.6
AlH ₂ Cl ↔ AlCl + H ₂ SP ^b	-1191	390	450	516	960	1837				4.0	75.6	79.6
AlH ₂ Cl ↔ AlH + HCl SP ^b	-1296	228	460	493	1341	1780				3.6	105	109
AlHCl + H ↔ AlH + HCl SP ^b	-1542	308	369	466	557	1724				3.3	84.9	88.2
AlHCl ₂	161	433	470	573	646	1924				27.7	225	253
AlCl + HCl ↔ AlHCl ₂ SP ^b	-1415	102	290	308	514	1385				35.9	248	284
AlCl + HCl ↔ AlCl ₂ + H SP ^b	-1275	113	285	309	429	524				29.0	245	274
AlCl ₃	146	146	198	376	612	612				226	226	452
AlCl ₂ + Cl ↔ AlCl + Cl ₂ SP ^b	-463	26	118	133	235	497				51	723	774
AlH ₄	470	566	568	626	778	1223	1433	1858	1877	5.2	6.9	9.8
AlH ₂ + H ₂ ↔ AlH ₃ + H SP ^b	-1503	247	268	739	772	853	941	1816	1836	3.9	12.6	16.5
AlH ₂ + H ₂ ↔ AlH ₄ SP ^b	-720	407	612	726	727	1378	1455	1869	1895	5.0	6.6	10.1
AlH ₃ + H ↔ AlH ₄ SP ^b	-438	272	444	665	725	741	1762	1844	1855	6.4	8.2	9.7
AlH ₃ Cl	330	414	494	512	640	773	1138	1445	1896	6.8	79.3	83.3
AlH ₂ Cl + H ↔ AlHCl + H ₂ SP ^b	-1516	155	246	509	558	732	839	971	1848	10.2	81.9	92.1
AlH ₂ + HCl ↔ AlH ₂ Cl + H SP ^b	-784	198	362	464	598	692	1450	1827	1862	5.9	109	111
AlH ₃ Cl ↔ AlHCl + H ₂ SP ^b	-1033	368	436	522	653	789	1236	1620	1915	6.5	79.0	84.1
AlH ₂ Cl + H ↔ AlH ₃ Cl SP ^b	-410	256	487	509	12	603	719	1757	1885	7.7	80.1	83.0
AlH ₂ Cl ₂	156	187	441	460	474	604	722	1081	1469	32.0	232	261
AlHCl ₂ + H ↔ AlCl ₂ + H ₂ SP ^b	-1512	152	153	156	458	581	683	799	1012	41.5	227	268
AlHCl ₂ + H ↔ AlHCl + HCl SP ^b	-1628	109	283	302	471	520	588	599	1857	35.3	244	276
AlH ₂ Cl ₂ ↔ AlCl ₂ + H ₂ SP ^b	-1408	148	369	383	455	604	742	873	1730	30.2	238	265
AlHCl ₂ + H ↔ AlH ₂ Cl ₂ SP ^b	-277	157	293	459	505	551	589	614	1742	33.0	231	259
AlCl ₃ + H ↔ AlCl ₂ + HCl SP ^b	-1485	92	120	169	294	362	429	540	584	233	255	478
AlHCl ₂ + H ↔ AlCl ₂ + HCl SP ^b	-400	36	60	142	378	433	583	584	633	232	457	688
AlCl ₄	90	131	144	149	213	243	344	530	599	356	409	508
H ₂	4140									0.28		
HCl	2845									1.6		
Cl ₂	499									72.0		

^a Vibrational frequencies computed at the QCISD/6-31G(d) level have been scaled by 0.9537, as recommended by Scott and Radom.²⁰ ^b SP indicates a first-order saddle point on the reaction path between the given reactant(s) and product(s).

calculation of the electronic energy at higher levels shifts this saddle point to an energy slightly lower than that of the addition complexes. Thus, there is no true energetic barrier to this reaction. This reaction should also be pressure-dependent, and in the low-pressure limit, chemically activated AlHCl produced from Al + HCl will decompose to AlCl + H before it can be collisionally stabilized. So at low pressures, this provides a barrierless path for the overall reaction Al + HCl → AlCl + H. The direct reaction path for Al + HCl → AlCl + H has an energetic barrier of about 4 kcal/mol. This is generally consistent with the kinetics observed by Rogowski et al.² In their experiments, both the direct reaction of Al + HCl to give AlCl + H and the reaction proceeding through chemically activated AlHCl may have been occurring. They did not observe any pressure dependence in their experiments from 12 to 40 Torr, but it is likely that the reaction proceeding through chemically activated AlHCl is in the low-pressure limit for these conditions, and in the low-pressure limit, its rate should be independent of pressure. The small positive activation energy measured by Rogowski et al. (1.6 kcal/mol) is between the value that would be expected for the direct abstraction with a 4 kcal/mol energetic barrier and the near-zero value that would be expected for the barrierless reaction proceeding through chemically activated AlHCl. So our results are generally consistent with the experi-

ments of Rogowski et al. A quantitative comparison between our calculations and their results would require detailed master equation treatment of the chemically activated process (with a variational selection of the transition state) in parallel with the direct abstraction reaction. AlH + Cl can react without an energetic barrier to give Al + HCl, AlCl + H, or AlHCl. The reaction to produce AlHCl is a simple radical recombination reaction. Barrierless paths for the other two reactions were identified on the basis of potential energy surface scans at the UHF/6-31G(d) level.

AlCl₂. The Al + Cl₂ reaction was studied experimentally by Rogowski et al.² They measured a rate constant of $7.9 \times 10^{-10} \exp(-780/T) \text{ cm}^3 \text{ molecule}^{-1} \text{ s}^{-1}$ for this process. Our computed AlCl₂ potential surface is summarized in Figure 2c. Both the addition reaction to give AlCl₂ and the Cl atom transfer reaction to give AlCl + Cl are predicted to be barrierless by calculations at the UHF/6-31G(d), UMP2(full)/6-31G(d), UB3LYP/6-31G(d), and UHF/6-311+G(3df,2p) levels of calculation. As a rule, the UHF and UMP2 calculations tend to overpredict barrier heights, so we do not expect that higher-level calculations would reveal an electronic energy barrier. Our computational results at first appear to be inconsistent with Rogowski et al.'s observation of

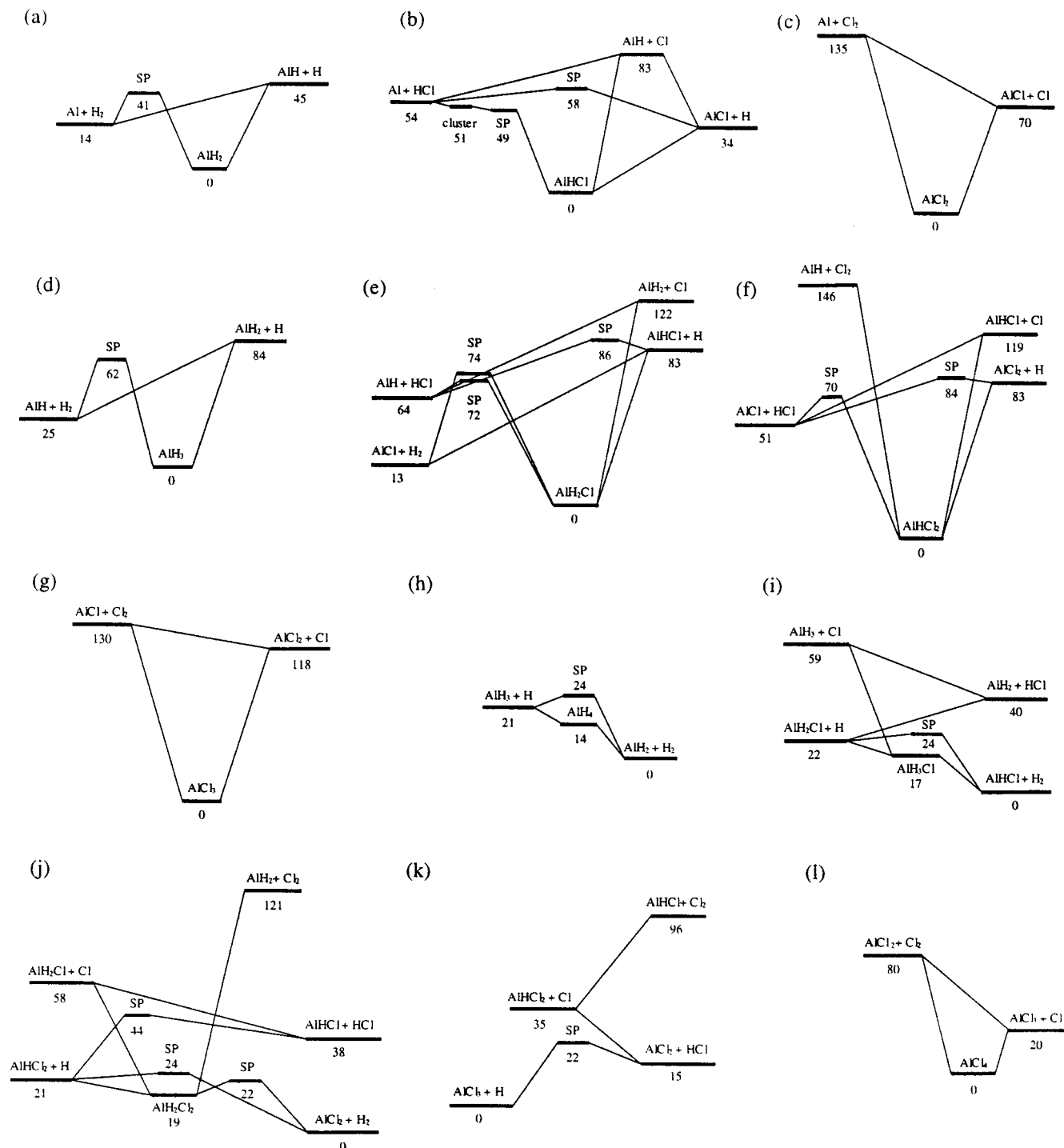


Figure 2. Schematic energy diagrams for the Al–H–Cl system. Energies are in kcal/mol at 0 K, are relative to the lowest-energy structure of each stoichiometry, and are based on calculations using the CBS-RAD method. SP indicates a first-order saddle point on the potential surface.

a positive activation energy for this reaction. However, as underlined by Dean and Bozzelli,²³ a temperature exponent of 1.5 is expected for an atom abstraction from a stable species by an atom. If this temperature exponent is held fixed, the experimental data can be fit by $1.23 \times 10^{-14} T^{1.5} \exp(+74/T)$ $\text{cm}^3 \text{ molecule}^{-1} \text{ s}^{-1}$ with accuracy comparable to that of the Arrhenius fit presented by Rogowski et al. Our prediction of a zero or slightly negative activation energy for this reaction is thus consistent with the experimental data when the expected temperature dependence of the pre-exponential factor is taken into account.

AlH₃. Our computed potential surface for AlH₃ is summarized in Figure 2d. Note that no CBS-Q or G-2 calculations were

possible for the $\text{AlH} + \text{H}_2 \leftrightarrow \text{AlH}_3$ transition state. The restricted Hartree–Fock wave function for this transition state had an RHF to UHF instability. The insertion of AlH into H₂ to give AlH₃ is predicted to have a substantial energetic barrier (about 37 kcal/mol). This is generally consistent with the experimental results of Pasternack and Rice,¹ who attempted to study this reaction at 300 K. They were unable to observe any reaction of AlH with H₂ but measured a rate constant near the lower limit of their experiment’s resolution for the reaction of AlH with D₂. On the basis of the lower detection limit of their experiments, they derived an upper limit of $10^{-14} \text{ molecule}^{-1} \text{ cm}^3 \text{ s}^{-1}$ for the bimolecular rate constant of the AlH + H₂ reaction. This suggests that there is a barrier of at least 7–10 kcal/mol

for this reaction but does not support or contradict the much larger barrier predicted by our calculations. If their measured rate constant for the Al + D₂ reaction of 1.4×10^{-14} molecule⁻¹ cm³ s⁻¹ at 460 Torr and 300 K in argon is correct, it would imply a barrier to reaction substantially smaller than the 37 kcal/mol predicted here. However, they state that their measured value is “near the limit of detectability of these experiments”, and we should not therefore rule out the possibility that the barrier to reaction is much larger than would be expected on the basis of that measurement. The AlH₂ + H ↔ AlH + H₂ reaction is predicted to be barrierless on the basis of scans of the potential energy surface. At the UHF/6-31G(d) level, there is a small barrier (about 2 kcal/mol) for this process, but at the UB3LYP/6-31G(d) and UMP2/6-31G(d) levels, barrierless paths from the reactants to products were identified.

AlH₂Cl. The computed potential surface for AlH₂Cl is shown schematically in Figure 2e. To our knowledge, reactions on this surface have not previously been studied experimentally or theoretically. For all three transition-state structures included in this diagram, the restricted Hartree–Fock wave function had an RHF to UHF instability, and the CBS-Q and G-2 methods were therefore not applied. Insertion of AlH into HCl is predicted to have a significant energetic barrier (about 8 kcal/mol), but insertion of AlCl into H₂ is predicted to have a much larger barrier (about 61 kcal/mol). From the point of view of AlH₂Cl decomposition, this means that although H₂ elimination is much more thermodynamically favorable than HCl elimination, HCl elimination has a smaller energetic barrier to reaction. HCl elimination also proceeds through a slightly “looser” transition state than H₂ elimination, as can be seen from the vibrational frequencies and moments of inertia for these transition states shown in Table 2. This situation is strikingly similar to the corresponding HCl and H₂ elimination reactions from SiH₂Cl₂.^{24–26} The two possible H-transfer reactions in this system, AlHCl + H ↔ AlCl + H₂ and AlH₂ + Cl ↔ AlH + HCl, are both predicted to be barrierless by potential energy surface scans, from which we identified barrierless reaction paths at the UHF/6-31G(d) level. The Cl-atom transfer reaction, AlHCl + H ↔ AlH + HCl, is predicted to have a small energetic barrier (about 3 kcal/mol).

AlHCl₂. The computed potential surface for AlHCl₂ is summarized in Figure 2f. The AlCl + HCl ↔ AlCl₂ + H reaction was studied experimentally by Slavejkov and Fontijn³, who measured the rate constant to be 1.1×10^{-11} exp(−13100K/T) cm³ molecule⁻¹ s⁻¹ between 1330 and 1610 K at total pressures of 30 to 80 mbar. They did not observe any pressure dependence of the reaction rate over this limited pressure range. Their experimental activation energy of about 26 kcal/mol is significantly smaller than our predicted energetic barrier of 33 kcal/mol for this bimolecular reaction. However, if some of the chemically activated AlHCl₂ that should also be formed from AlCl + HCl was either being collisionally stabilized or decomposing to AlCl₂ + H rather than back to the reactants, the apparent activation energy would be lowered. Our predicted energetic barrier for AlCl + HCl ↔ AlHCl₂ is about 19 kcal/mol. It should also be noted that their measured activation energy is substantially smaller than the endothermicity for AlCl + HCl ↔ AlCl₂ + H predicted by our calculations. The H-atom transfer from AlHCl to Cl is predicted to be barrierless. A barrierless path for this reaction was identified on the basis of potential energy surface scans at the UHF/6-31G(d) level of calculation. The insertion of AlH into Cl₂ is predicted to occur without a barrier on the basis of the large exothermicity of this reaction. However, we were unable to identify either a well-defined

transition state or a barrierless path for this reaction at the UHF/6-31G(d), UMP2/6-31G(d), and UB3LYP/6-31G(d) levels of calculation. Potential surface scans at these levels produced surfaces that were not smooth but that had apparent discontinuities in slope. In constructing these surfaces, we took great care to ensure that the wave function at each geometry was stable with respect to small perturbations. In many cases, the calculations first converged to wave functions with instabilities. In these scans, the Al–Cl distance and Cl–Cl distance were scanned, while the Al–H distance was held fixed and the geometry was restricted to C_{2v} symmetry. It is not clear whether the apparent discontinuities would disappear if these restrictions were removed.

AlCl₃. The potential surface for AlCl₃ is summarized in Figure 2g. The AlCl + Cl₂ → AlCl₂ + Cl reaction was studied experimentally by Rogowski et al.² Their measured rate constant for this reaction for temperatures from 400 to 1025 K was 9.6×10^{-11} exp(−610K/T) cm³ molecule⁻¹ s⁻¹. At the UHF/6-31G(d) and QCISD/6-31G(d) levels of calculation, an energetic barrier is predicted for this reaction, while at the UB3LYP/6-31G(d) level, a scan of the potential surface shows the reaction to be barrierless. When the energies are computed at higher levels and with larger basis sets and when the zero-point energy is included, the saddle point found at the UHF/6-31G(d) and QCISD/6-31G(d) levels is substantially lower in energy than AlCl + Cl₂. As shown in Table 1, at the CBS-RAD level of calculation, this point is 8 kcal/mol lower in energy than the separated reactants. So our calculations lead us to conclude that this reaction is barrierless. As was the case for the Al+Cl₂ reaction, our results at first appear to be inconsistent with the positive activation energy measured by Rogowski et al. According to Dean and Bozzelli,²³ a temperature exponent near 2 is expected for an atom abstraction from a stable species by a diatomic radical. The experimental data can be fit well by $3.28 \times 10^{-17} T^2$ exp(+574/T) cm³ molecule⁻¹ s⁻¹ with an accuracy similar to that obtained with the Arrhenius fit given by Rogowski et al. Our prediction of a negative activation energy for this reaction is therefore consistent with the experimental data. The insertion of AlCl into Cl₂ is predicted to occur without a barrier on the basis of the large exothermicity of this reaction. However, we were unable to identify either a well-defined transition state or a barrierless path for this reaction at the UHF/6-31G(d), UMP2/6-31G(d), and UB3LYP/6-31G(d) levels of calculation. The situation was identical to that described above for the insertion of AlH into Cl₂.

AlH₄. The computed potential surface for AlH₄ is shown schematically in Figure 2h. We are not aware of any previous experimental or theoretical studies of these reactions. At the UHF/6-31G(d), MP2/6-31G(d), and QCISD/6-31G(d) levels of calculation, AlH₄ is a local minimum on the potential surface, and a transition state for its decomposition to AlH₂ + H₂ can be identified. However, as shown in Table 1, when the energies are computed at higher levels and with larger basis sets and when the zero-point energy is included, this transition state becomes lower in energy than AlH₄. Thus this reaction is barrierless. The AlH₃ + H → AlH₄ reaction is not a simple radical recombination, since AlH₃ is a closed-shell molecule. Therefore, we cannot simply assume that this reaction is barrierless. At the UHF/6-31G(d) and MP2/6-31G(d) levels of calculation, a barrier is predicted. However, these levels of calculation also predict that this reaction is exothermic rather than endothermic, as predicted by higher-level calculations. Calculations at the UB3LYP/6-31G(d) level correctly predict that the reaction is exothermic. A potential surface scan at this

level predicts that there is no energetic barrier for this reaction. Calculations at the UQCISD/6-31G(d) level also correctly predict that the reaction is exothermic, but they do predict a barrier. As shown in Table 1, when the energies are computed at higher levels and with larger basis sets and when the zero-point energy is included, this transition state becomes slightly lower in energy than the reactants. Therefore, we also predict that this reaction is barrierless. Combined with the barrierless decomposition of AlH_4 to $\text{AlH}_2 + \text{H}_2$, this provides a rather indirect but barrierless reaction path for the overall reaction $\text{AlH}_3 + \text{H} \rightarrow \text{AlH}_2 + \text{H}_2$. As shown in Table 1 and Figure 2, a direct reaction path for $\text{AlH}_3 + \text{H} \rightarrow \text{AlH}_2 + \text{H}_2$ was also identified, with an energetic barrier of about 3 kcal/mol.

AlH_3Cl . The computed potential surface for AlH_3Cl is shown schematically in Figure 2i. It is similar to that for AlH_4 . At the UHF/6-31G(d), MP2/6-31G(d), and QCISD/6-31G(d) levels of calculation, AlH_3Cl is a local minimum on the potential surface, and a transition state for its decomposition to $\text{AlHCl} + \text{H}_2$ can be identified. However, as shown in Table 1, when the energies are computed at higher levels and with larger basis sets and when zero-point energy is included, this saddle point becomes approximately equal in energy to AlH_3Cl . Thus this reaction has no significant energetic barrier. The $\text{AlH}_2\text{Cl} + \text{H} \rightarrow \text{AlH}_3\text{-Cl}$ reaction is also predicted to be barrierless. At the UHF/6-31G(d), MP2/6-31G(d), and QCISD/6-31G(d) levels of calculation, a barrier is predicted for this reaction. However, these levels of calculation also predict that this reaction is exothermic rather than endothermic, as predicted by higher-level calculations. Calculations at the UB3LYP/6-31G(d) level correctly predict that the reaction is exothermic. A potential surface scan at this level predicts that there is no energetic barrier for this reaction. As shown in Table 1, when the energies are computed at higher levels and with larger basis sets and when the zero-point energy is included, this saddle point becomes lower in energy than the reactants. Therefore, we also predict that this reaction is barrierless. Combined with the barrierless decomposition of AlH_3Cl to $\text{AlHCl} + \text{H}_2$, this provides a barrierless reaction path for the overall reaction $\text{AlH}_2\text{Cl} + \text{H} \rightarrow \text{AlHCl} + \text{H}_2$. As shown in Table 1 and Figure 2, a direct reaction path for $\text{AlH}_2\text{Cl} + \text{H} \rightarrow \text{AlHCl} + \text{H}_2$ was also identified, with an energetic barrier of about 2 kcal/mol. The Cl-atom transfer reaction $\text{AlH}_2 + \text{HCl} \rightarrow \text{AlH}_2\text{Cl} + \text{H}$ has a small energetic barrier and well-defined saddle point on the reaction path at the UHF/6-31G(d), MP2/6-31G(d), B3LYP/6-31G(d), and QCISD/6-31G(d) levels. However, when the zero-point energy is included and when the energies are calculated at higher levels of theory and with larger basis sets, this saddle point becomes slightly lower in energy than the reactants. Thus, this reaction is also predicted to be barrierless. The association reaction $\text{AlH}_3 + \text{Cl} \rightarrow \text{AlH}_3\text{Cl}$ is predicted to be barrierless by scans of the potential energy surface at the UB3LYP/6-31G(d) level. At the UHF/6-31G(d) and UMP2/6-31G(d) levels, we were unable to find either a saddle point connecting the reactants and products or a barrierless path connecting them. However, on the basis of the UB3LYP/6-31G(d) results, we predict that this reaction is barrierless. The H-atom transfer reaction $\text{AlH}_3 + \text{Cl} \rightarrow \text{AlH}_2 + \text{HCl}$ was found to be barrierless on the basis of scans of the potential energy surface at the UHF/6-31G(d) level.

AlH_2Cl_2 . The computed potential surface for AlH_2Cl_2 is summarized in Figure 2i. AlH_2Cl_2 is a first-order saddle point at the UHF/6-31G(d) level of theory but a local minimum at the UB3LYP/6-31G(d), UMP2/6-31G(d), and UQCISD/6-31G(d) levels of theory. Its decomposition to $\text{AlCl}_2 + \text{H}_2$ is predicted to have an energetic barrier at all of the levels of theory

considered here. This barrier is about 3 kcal/mol at the CBS-RAD level of calculation. At the UHF/6-31G(d) level, where AlH_2Cl_2 is a first-order saddle point, the imaginary frequency corresponds to the decomposition of AlH_2Cl_2 to $\text{AlHCl}_2 + \text{H}$. The $\text{AlHCl}_2 + \text{H}$ association reaction that forms AlH_2Cl_2 is predicted to be endothermic by calculations at the UHF/6-31G(d), UMP2/6-31G(d), and UQCISD/6-31G(d) levels. However, it is predicted to be exothermic by calculations at the UB3LYP/6-31G(d) level, as well as by the higher-level calculations whose results are shown in Table 1. At the UHF/6-31G(d) level, this reaction is predicted to be barrierless, while at the UMP2/6-31G(d) and UQCISD/6-31G(d) levels, it has a barrier, and a transition state for the reaction was located. As shown by the CBS-RAD calculation in Table 1, however, when higher-level methods are used, this saddle point becomes slightly lower in energy than the reactants. As was the case for the analogous reactions in the AlH_4 and AlH_3Cl systems, this reaction is predicted to be barrierless. The direct H-atom transfer reaction $\text{AlHCl}_2 + \text{H} \rightarrow \text{AlCl}_2 + \text{H}$ is predicted to have about a 3 kcal/mol energetic barrier. However, the H-atom transfer reaction $\text{AlH}_2\text{Cl} + \text{Cl} \rightarrow \text{AlHCl} + \text{HCl}$ is predicted to be barrierless on the basis of potential energy surface scans at the UHF/6-31G(d) level. The Cl-atom transfer reaction $\text{AlHCl} + \text{HCl} \rightarrow \text{AlHCl}_2 + \text{H}$ is predicted to have approximately a 6 kcal/mol energetic barrier. The association reaction $\text{AlH}_2\text{Cl} + \text{Cl} \rightarrow \text{AlH}_2\text{Cl}_2$ is predicted to be barrierless. At the UHF/6-31G(d) and UMP2/6-31G(d) levels, we were unable to find either a saddle point or a barrierless path connecting the reactants and products. However, at the UB3LYP/6-31G(d) level, a barrierless reaction path was identified. The situation was the same for the $\text{AlH}_2 + \text{Cl}_2 \rightarrow \text{AlH}_2\text{Cl}_2$ insertion reaction. At the UHF/6-31G(d) and UMP2/6-31G(d) levels, we were unable to find either a saddle point connecting the reactants and products or a barrierless path connecting them. However, at the UB3LYP/6-31G(d) level, a barrierless reaction path was identified.

AlHCl_3 . The computed potential surface for AlHCl_3 is summarized in Figure 2k. In contrast to the other $\text{AlH}_x\text{Cl}_{4-x}$ species, AlHCl_3 is not a local minimum on the potential energy surface for any of the methods applied here. The Cl-atom transfer reaction $\text{AlCl}_2 + \text{HCl} \rightarrow \text{AlCl}_3 + \text{H}$ is predicted to have a significant energetic barrier of about 7 kcal/mol. However, the Cl-atom transfer reaction $\text{AlHCl} + \text{Cl}_2 \rightarrow \text{AlHCl}_2 + \text{Cl}$, which is much more exothermic, is predicted by potential energy surface scans at the UHF/6-31G(d) level to be barrierless. The H-atom transfer reaction $\text{AlHCl}_2 + \text{Cl} \rightarrow \text{AlCl}_2 + \text{HCl}$ has an energetic barrier and a well-defined saddle point on the reaction path at the UHF/6-31G(d), UMP2/6-31G(d), UB3LYP/6-31G(d), and UQCISD/6-31G(d) levels of calculation. However, when zero-point energy is included and when the energies are calculated at higher levels of theory and with larger basis sets, this saddle point becomes slightly lower in energy than the reactants. Thus, this reaction is also predicted to be barrierless.

AlCl_4 . The computed potential surface for AlCl_4 is summarized in Figure 2l. AlCl_4 is predicted by the higher-level calculations to be a stable structure approximately 20 kcal/mol lower in energy than $\text{AlCl}_3 + \text{Cl}$. Its formation from $\text{AlCl}_3 + \text{Cl}$ is predicted to occur without an energetic barrier by potential surface scans at the UHF/6-31G(d) level. At this level, however, the UHF/6-31G(d) calculations predict that AlCl_4 is a first-order saddle point, about 6 kcal/mol higher in energy than $\text{AlCl}_3 + \text{Cl}$. The Cl-atom transfer reaction $\text{AlCl}_2 + \text{Cl} \rightarrow \text{AlCl}_3 + \text{Cl}$ has a small energetic barrier of 2.6 kcal/mol at the UHF/6-31G(d) level. However, at the UMP2/6-31G(d) level, where a first-

order saddle point could also be identified, the saddle point was 0.2 kcal/mol lower in energy than the reactants. We have not carried out higher levels of calculation because of computational expense and difficulties in locating this saddle point on the extremely flat potential surface (the imaginary frequency at the UMP2/6-31G(d') saddle point was only 42 cm⁻¹). However, since the UHF and UMP2 calculations tend to overestimate barrier heights in general, we can safely conclude that there is no energetic barrier to this reaction. Our calculations for the insertion of AlCl₂ into Cl₂ to give AlCl₄ gave results similar to those for the insertion of AlH and AlCl into Cl₂. We were unable to locate either a well-defined transition state or a completely barrierless path from AlCl₂ + Cl₂ to AlCl₄. Again there were apparent discontinuities in the slope of the potential energy surface when the Al–Cl and Cl–Cl bond lengths were varied holding other bond lengths and angles fixed. However, a nonsmooth path from AlCl₂ + Cl₂ to AlCl₄ was found with a maximum energy only about 4 kcal/mol above that of AlCl₂ + Cl₂ at the UHF/6-31G(d) level. It is likely that at higher levels of calculation and with no bond lengths or angles constrained, this apparent barrier would disappear, as we have observed for many of the other reactions studied here. We therefore predict that this reaction is barrierless as well, though we have not actually shown that to be the case.

Summary and Conclusions

High-level ab initio quantum chemical calculations have been used to investigate possible reactions in the Al–H–Cl system. Transition states or barrierless reaction paths have been identified for essentially all feasible reactions in this system involving a single aluminum atom. These results provide a basis for the estimation of reaction rate parameters for this system using transition state theory and related unimolecular reaction rate theories, thereby constructing a reaction mechanism useful for detailed chemical kinetic modeling of aluminum combustion in HCl and chemical vapor deposition processes using AlCl₃ in H₂. In the few cases where previous experimental or theoretical results have been published, the present work is consistent with previous work.

Acknowledgment. This research was partially supported by generous grants of computer time from the University at Buffalo (SUNY) Center for Computational Research, which are grate-

fully acknowledged. L.C. wishes to thank Dr. Pierre Florian from CRMHT-CNRS, Orleans, for valuable discussions.

References and Notes

- (1) Rogowski, D. F.; Marshall, P.; Fontijn, A. *J. Phys. Chem.* **1989**, *93*, 1118–1123.
- (2) Pasternack, L.; Rice, J. K. *J. Phys. Chem.* **1991**, *95*, 8701–8706.
- (3) Slavejkov, A. G.; Fontijn, A. *Chem. Phys. Lett.* **1990**, *165*, 375–378.
- (4) Sakai, S. *J. Phys. Chem.* **1992**, *96*, 8369–8373.
- (5) Fångström, T.; Lunell, S.; Kasai, P. H.; Eriksson, L. A. *J. Phys. Chem. A* **1998**, *102*, 1005–1017.
- (6) Swihart, M. T.; Catoire, L. *Combust. Flame* **2000**, *121*, 210–222.
- (7) Catoire, L.; Swihart, M. T.; Legrand, B.; Gökalp, I.; Paillard, C. *Combust. Flame*, submitted for publication.
- (8) Becke, A. D. *Phys. Rev. A* **1988**, *38*, 3098.
- (9) Lee, C.; Yang, W.; Parr, R. G. *Phys. Rev. B* **1988**, *37*, 785.
- (10) Becke, A. D. *J. Chem. Phys.* **1993**, *98*, 5648.
- (11) Ochterski, J. W.; Petersson, G. A.; Wiberg, K. B. *J. Am. Chem. Soc.* **1995**, *117*, 11299–11308.
- (12) Curtiss, L. A.; Raghavachari, K.; Trucks, G. W.; Pople, J. A. *J. Chem. Phys.* **1991**, *94*, 7221–7230.
- (13) Curtiss, L. A.; Raghavachari, K.; Pople, J. A. *J. Chem. Phys.* **1993**, *98*, 1293–1298.
- (14) Curtiss, L. A.; Redfern, P. C.; Smith, B. J.; Radom, L. *J. Chem. Phys.* **1996**, *104*, 5148–5152.
- (15) Frisch, M. J.; Trucks, G. W.; Schlegel, H. B.; Gill, P. M. W.; Johnson, B. G.; Robb, M. A.; Cheeseman, J. R.; Kieth, T.; Petersson, G. A.; Montgomery, J. A.; Raghavachari, K.; Al-Laham, M. A.; Zakrzewski, V. G.; Ortiz, J. V.; Foresman, J. B.; Cioslowski, J.; Stefanov, B. B.; Nanayakkara, A.; Challacombe, M.; Peng, C. Y.; Ayala, P. Y.; Chen, W.; Wong, M. W.; Andres, J. L.; Replogle, E. S.; Gomperts, R.; Martin, R. L.; Fox, D. J.; Binkley, J. S.; Defrees, D. J.; Baker, J.; Stewart, J. P.; Head-Gordon, M.; Gonzalez, C.; Pople, J. A. *Gaussian 94*, Revision E.2; Gaussian, Inc.: Pittsburgh, PA, 1995.
- (16) Mayer, P. M.; Parkinson, C. J.; Smith, D. M.; Radom, L. *J. Chem. Phys.* **1998**, *108*, 604–615.
- (17) Chuang, Y.-Y.; Coitino, E. L.; Truhlar, D. G. *J. Phys. Chem. A* **2000**, *104*, 446–450.
- (18) Allendorf, M. D.; Melius, C. F. *Proc. Electrochem. Soc.* **1999**, *98-23*, 28–33.
- (19) Allendorf, M. D.; Melius, C. F.; Bauschlicher, C. W., Jr. *J. Phys. IV (France)* **1999**, *9*, 23–31.
- (20) Scott, A. P.; Radom, L. *J. Phys. Chem.* **1996**, *100*, 16502–16513.
- (21) Senger, S.; Radom, L. *J. Phys. Chem. A* **2000**, *104*, 7375–7385.
- (22) Chase, M. W., Jr. *J. Phys. Chem. Ref. Data* **1998**, *Monograph 9*, 1–1951.
- (23) Dean, A. M.; Bozzelli, J. W. In *Gas-Phase Combustion Chemistry*; Gardiner, W. C., Jr., Ed.; Springer-Verlag: New York, 2000; pp 125–341.
- (24) Su, M.-D.; Schlegel, H. B. *J. Phys. Chem.* **1993**, *97*, 9981–9985.
- (25) Wittbrodt, J. M.; Schlegel, H. B. *Chem. Phys. Lett.* **1997**, *265*, 527–531.
- (26) Swihart, M. T.; Carr, R. W. *J. Phys. Chem. A* **1998**, *102*, 1542–1549.